Stability of Graphene/H_2O Nanoliquid flow on a Stretching/Contracting Wedge and Stagnation Point: A Solar Thermal Energy Application

Sangapatnam Suneetha
Department of Applied Mathematics
Yogi Vemana University,Kadapa-516005, India.
Corresponding Author E-Mail: ***suneethayvu@gmail.com***

ABSTRACT

Objectives: Boundary value issues occasionally offer a dual solution, one of which is really trustworthy and stable while the other is unstable. The intention of the current research is to use the Casson model to explain the double solutions of graphene/water nanofluid flow through a stretching or compressing wedge and stagnation point. For a specific range of the suction/injection parameter and the extending/contracting parameter, two solutions are found. **Methods:** The fluid transport equations are then converted into ordinary differential equations by applying the apt self-similarity variables and are computed using MATLAB's bvp4c. Graphs are used to show how certain factors affect the flow field.

Findings: The results of the current research shows that the permeability constraint on velocity and thermal variations obtained from the primary and secondary solutions are contrary in nature. The suction/injection parameter and skin friction are directly related for the first solution, whereas a contrary for other. The magnetic parameter reduces the temperature for the initial solution in both cases. According to the stability analysis, the second option is reliable.

Novelty and applications: These types of research may be helpful in the detection of glucose and cholesterol as well as in the development of Nano biosensors, targeted therapies, antifungal activity, anticancer, and cancer cell detection technologies. Reduced carbon dioxide emissions and energy consumption are two of the many benefits of using nanoparticles in thermal transmission fluid in solar collectors. Nanoparticles may also be used in a variety of inserts for solar energy systems, such as baffles, wire coils, generators, Wedge-shaped solar cookers, and twisted tapes.

KEYWORDS: Nanofluid, Casson Model, Graphene nanoparticle, dual solution,

Stability test

INTRODUCTION:

Currently, the world's population raise and industrial advancements are increasing the need for energy. The environment, the state of the economy, and respective living standards are all directly impacted by the problems relating to energy generation. Generally, as social and economic conditions improve and economic growth occurs, the energy consuming rises too. As a

result, countries are looking for alternatives that are appropriate to their circumstances, like population growth and societal type, as well as economic progress. Potentially useful replacements for fossil fuels include renewable energy sources including wind, solar, geothermal, and biomass. Some of them can be found easily, need little training, and provide good value. Solar energy has been discovered as an enormous source of energy among renewable energy sources. Solar energy harvesting has no negative effects on the environment. Furthermore, this energy source is appropriate for village, industrial, and building systems. As a result, this form of energy has recently received significant attention. One significant opportunity for research in the topic is the harvesting of solar energy via a high-performance pathway. Typically, systems being used storing or converting solar thermal energy have poor performance, which poses a difficulty to system designers. As a result, numerous studies have been done to optimize the capabilities of these systems.

However, magnetohydrodynamics (MHD) combines fluid dynamics and electromagnetism to examine how magnetic fields interact with electrically conducting liquids. Due to its significance in a wide variety of engineering and manufacturing applications, such as the petrochemical sector, MHD power generators, plasma training, nuclear reactors, and boundary layer control in aerodynamics, magnetic mixers, a lot of research has recently been concentrated on the study of MHD flow. Here, a number of recent research that examined the impact of MHD on flow and heat transfer issues are discussed. They typically considered liquid metals, water combined with other industrial fluids in the presence of a magnetic force to find the thermal conduction of a viscous and incompressible liquid passing over a variety of geometries. [1–6].

Fluids with shear-dependent viscosity and shear-thinning/shear-thickening properties are known as non-Newtonian fluids. Numerous industrial uses exist for these fluids, including those related to the production of petroleum, chemical processing, polymers made by plastic, methods to preserve food, cosmetic products, and the making of optical fibres. The flow characteristics of non-Newtonian fluids cannot be explained by the Navier-Stokes equations because they have complicated rheological characteristics. As a result, several researchers have proposed many models such as Casson model, Maxwell fluid model, Williamson fluid model, Cross fluid model, and Carreau fluid model. Several scholars explored into the transport properties of several non-Newtonian fluid models [7-9]. Casson fluid is one of the non-Newtonian fluid subclasses named

after Casson [10]. When the Casson fluid parameter is near zero, the model fluid is highly viscous, whereas near infinity, the viscosity drops dramatically. Additionally, this model may represent solid properties when shear stress is lower than yield stress and liquid qualities when shear stress is higher than yield stress, which is how shear-thinning behaviour occurs in nature. Because of its importance in defining the rheological behaviour of human being blood, ointment, honey, and ketchup, the Casson fluid model has garnered considerable attention. Mythili and Sivaraj [11] investigated unsteady Casson fluid flow across two distinct geometries using unequal energy gain/loss and discovered that the fluid velocity grows with the Casson fluid parameter.

It has drawn a lot of interest to employ nanofluids instead of usual fluids like H_2O, acetone, oil, ethylene glycol to improve thermal dissipation. A common fluid is used to suspend a solid phase that is nanoscale in a nanofluid. It is significant to note that one of the key components of a nanofluid is thermal conductivity. Generally, normal fluids have low heat conductivity characteristics, resulting in minimum transfer of heat to the thermal systems. However, as nano-dimension solid components have a great thermal conductivity, nanofluids have a larger potential to improve the thermal characteristics. The nanofluid is widely used in a variety of industries, including solar energy, biomedicine, nuclear reactors, drug targeting, electronic equipment cooling, cancer treatment, microelectronics, and radiator cooling for engines. Researchers have proposed a variety of nanofluid models in [12–17]. The fluid transport features in the Buongiorno [18] model are examined using thermophoretic diffusivity and Brownian motion. Further, nanofluids in different phases are explored in refs. [19–22].

Intense synchronous interest has been shown in the study of flow and heat transmission via wedge-shaped structures in both the engineering and chemical industries over the past several years. For instance, in the study of geothermal systems, thermal insulation, heat exchangers, ground water contamination, aerodynamics, hydrodynamics, and other related topics. Enhanced oil recovery, aircraft responses to atmospheric gusts, packed bed reactor geothermal enterprises, ground water contamination, and other uses also typically include such flows. To put it simply, a wedge is a movable inclined plane and one of the six triangular classical basic machines. It has the ability to separate two things or sections of an object, lift something up, or hold something in position. It transforms lateral force into transverse splitting force. Recently, some investigators [23-26] investigated wedge-shaped geometries with varying fluid fluxes.

Stagnation point flow, which occurs on all stationary objects that move in a fluid, is the term used to describe the fluid movement close to the stagnation zone in the vicinity of the blunt-nosed object. Heimanz [27] was the first to study the flow of a stagnation point in two dimensions. Several researchers are now investigating the stagnation point flow in a wide range of contexts, such as viscous and inviscid fluid flows [28–29], forward or backward, normal or oblique. These fluxes are particularly important for cooling electronic equipment, metallurgical operations, cooling nuclear reactors during emergency shutdowns, and paper manufacture. Numerous academics [30–32] have thought deeply about stagnation point flow and its futility.

A continuous solid phase with numerous voids or pores is referred to as a porous media. Nowadays, it has great industrial applications in engineering, oil recovery, ground water hydrology, medicine, coal ignition, misappropriation of dispersed stuff underground, etc. The study and design of heat exchangers can benefit from consideration of heat transport and porous media. Additionally, porous media is utilised to either heat or cool fluids and enhance thermal conductivity. Later on, a number of researchers [33–36] looked into the porous flows using various parameters.

The fundamental objective of this problem is to show that the flow of a nanofluid can be stable despite the existence of viscous dispersion and heat generation/absorption, as predicted by the Casson model. Permeability is also taken into consideration. To evaluate the worth of the *Pr* for any fluid, the self-similarity quantities have been acquired. An exhaustive literature search reveals that the dual nature and stability of the nanofluid spanning two different geometries in the heat generation and absorption spectrum with the Casson model has not been investigated.

The present effort seeks to answer the very next research questions in light of the effects of these kinds of issues:

I. When extending or contracting two shapes, how many solutions result?
II. Which of the found solutions is stable and physically attainable?
III. How does the rate of thermal transfer a Casson nanofluid flow vary between two various geometries?
IV. How do heat generation/absorption, porosity, and viscous dissipation affect temperature and velocity?

The bvp4c collocation algorithm in MATLAB is used to numerically solve the system of fluid motion equations. It is noted that there are two solutions for the stagnation point as well as the expanding/contracting wedge. To confirm the stability of dual solutions, a stability test is executed. Contour plots and 2-dimensional plots are used to demonstrate how the active parameters affect the results.

2. MATHEMATICAL FORMULATION

A steady convective MHD flow of Graphene/H_2O nanofluid over a permeable extending/contracting stagnation point and wedge in two-dimensional with casson model is taken into account, and is exhibited in Fig.1. The velocity outside the boundary layer is $u_\infty = bx^m$, b is constant. The Hartree pressure gradient $m = \frac{\beta_1}{2-\beta_1}$, $\beta_1 = 0.5$ for a wedge and $\beta_1 = 1.0$ for stagnation point of a flat surface . A constant temperature of the wall (T_w) which is larger than the ambient temperature (T_∞). The thermophysical properties of Graphene /H_2O hybrid nanoliquid are revealed in Table.1. The rheological equation of form for an isotropic and non-compressible Casson fluid flow is assumed to be as follows (Mukhopadhyay [37] , Pramanik [38]):

$$\tau_{ij} = \begin{cases} 2\left(\mu_B + P_y \big/ \sqrt{2\pi}\right) e_{ij}, & \pi > \pi_c \\ 2\left(\mu_B + P_y \big/ \sqrt{2\pi_c}\right) e_{ij}, & \pi < \pi_c \end{cases}$$

where μ_B is the dynamic viscosity of the non-Newtonian fluid, P_y is the fluids yield stress, $\pi = e_{ij} e_{ij}$, e_{ij} is the $(i, j)^{th}$ constituent of the deformation rate and π_c is the critical value.

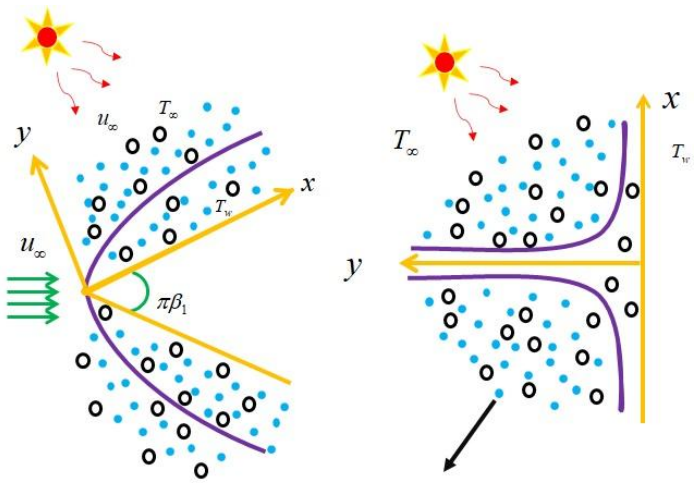

Fig.1 Graphene –Water nanofluid

The governing equations are:

$$\frac{\partial u}{\partial x}+\frac{\partial v}{\partial y}=0 \tag{1}$$

$$u\frac{\partial u}{\partial x}+v\frac{\partial u}{\partial y}=u_\infty\frac{du_\infty}{dx}+\frac{\mu_{nf}}{\rho_{nf}}\left(1+\frac{1}{\beta}\right)\left(\frac{\partial^2 u}{\partial y^2}\right)-\frac{\nu_{nf}}{K_1}(u-u_\infty)-\frac{\sigma_{nf}B_0^2}{\rho_{nf}}(u-u_\infty) \tag{2}$$

$$u\frac{\partial T}{\partial x}+v\frac{\partial T}{\partial y}=\frac{k_{nf}}{(\rho C_p)_{nf}}\frac{\partial^2 T}{\partial y^2}+\frac{\mu_{nf}}{(\rho C_p)_{nf}}\left(1+\frac{1}{\beta}\right)\left(\frac{\partial u}{\partial y}\right)^2+\frac{Q_0}{(\rho C_p)_{nf}}(T-T_\infty) \tag{3}$$

The Boundary conditions are

$$\begin{aligned} &u=\lambda_M u_\infty,\ v=V_w,\ T=T_w \ \text{ at } \ y=0,\\ &u=u_\infty,\ T\to T_\infty \qquad \text{as } \ y\to\infty \end{aligned} \tag{4}$$

Indicators of self-similarity that can be used are:

$$\begin{aligned} &\eta=\left(\frac{y}{x}\right)\lambda,\quad f(\eta)=\frac{\psi(x,y)}{\alpha^*\lambda},\ u=\quad f'(\eta)bx^m(1+\mathrm{Pr})^{-2n}\\ &v=-\left(\frac{\alpha^*}{x}\right)\lambda\ \left[f(\eta)(m+1)(0.5)+\eta f'(\eta)(m-1)(0.5)\right]\\ &V_w=-\left(\frac{\alpha^*}{x}\right)\lambda\ (m+1)f_w(0.5), T=(T_w-T_\infty)\theta(\eta)+T_\infty. \end{aligned} \tag{5}$$

By implanting the equation (5), Equs. (2)-(3) are converted to

$$\Pr f'''\left(1+\frac{1}{\beta}\right)A1+f\,f''(m+1)(0.5)+m\left((1+\Pr)^{4n}-(f')^{2}\right)$$
$$-K_a A1\left(f'(1+\Pr)^{2n}-(1+\Pr)^{4n}\right)-\frac{\sigma_{nf}}{\sigma_f}\frac{M_a}{A2}\left(f'(1+\Pr)^{2n}-(1+\Pr)^{4n}\right)=0 \tag{6}$$

$$\frac{k_{nf}}{k_f}\frac{1}{A3}\theta''+\left(\frac{m+1}{2}\right)f\theta'+\frac{\Pr E_c\left(f''\right)^{2}}{(1+\Pr)^{2n}A4}\left(1+\frac{1}{\beta}\right)+\frac{Q\theta}{A3}(1+\Pr)^{2n}=0 \tag{7}$$

As a result of the altered border conditions

$$f(\eta)=f_w,\quad f'(\eta)=\lambda_M(1+\Pr)^{2n},\ \theta(\eta)=1\ \text{ at } \eta=0,$$
$$f'(\eta)=(1+\Pr)^{2n},\quad \theta(\eta)\to 0,\qquad \text{as } \eta\to\infty. \tag{8}$$

Where

$$A1=\frac{1}{(1-\phi_1)^{2.5}\left((1-\phi)+\phi\left(\frac{\rho_s}{\rho_f}\right)\right)},\ A2=\left((1-\phi)+\phi\left(\frac{\rho_s}{\rho_f}\right)\right)$$
$$A3=\left((1-\phi)+\phi\left(\frac{(\rho C_p)_s}{(\rho C_p)_f}\right)\right),\ A4=\left((1-\phi)^{2.5}\right)\left((1-\phi)+\phi\left(\frac{(\rho C_p)_s}{(\rho C_p)_f}\right)\right) \tag{9}$$

$$\frac{k_{nf}}{k_f}=\frac{k_s+2k_f-2\phi(k_f-k_s)}{k_s+2k_f+\phi(k_f-k_s)}\qquad \sigma_{nf}=\sigma_f\left(\frac{3\left(\frac{\sigma_s}{\sigma_f}-1\right)\phi}{\left(\frac{\sigma_s}{\sigma_f}+2\right)-\phi\left(\frac{\sigma_s}{\sigma_f}-1\right)}+1\right) \tag{10}$$

$$\Pr=\frac{\mu_f(Cp)_f}{k_f},K_a=\frac{K_1 b x^{m-1}}{\nu_f},M_a=\frac{\sigma_f B_0^2 b x^{m-1}}{\nu_f},E_c=\frac{u_\infty^2}{C_p(T_w-T_\infty)},Q=\frac{Q_0}{bx^m(\rho C_p)_f} \tag{11}$$

Lin and Lin [39] have launched a metric $\lambda=\sqrt{\mathrm{Re}}\,\delta$ that may be used to assess the value of any fluid's worth , $\mathrm{Re}=U_\infty x\upsilon^{-1}$ is Reynolds number, $\delta=(1+\Pr)^{-n}\sqrt{\Pr},\ n=1/6$ for wedge($\beta_1=0.5$) and stagnation point plate $\beta_1=1.0$.

The heat transfer coefficient and dimensionless skin friction factor are stated as follows:

$$C_f^* \mathrm{Re}^{1/2} = \frac{2 f''(0)\sqrt{\mathrm{Pr}}}{(1-\phi)^{2.5}\sqrt{1+\mathrm{Pr}}}$$
$$Nu^* \mathrm{Re}^{1/2}\delta^{-1} = -\frac{k_{nf}}{k_f}\theta'(0). \tag{12}$$

Table 1: Graphene nanoparticles and the base fluid's thermophysical characteristics are tabulated below.

Physical Properties	Graphene	Water
ρ / kgm^{-3}	2250	997
$c_p / Jkg^{-1}K^{-1}$	2100	4197
$k / Wm^{-1}K^{-1}$	2500	0.613
σ / Sm^{-1}	10^7	0.005

Stability Check: Following the results of Bachok et al. [40] and Makinde [41], we conduct a stability test and find that the second set of solutions is robust whereas the first set is not. Thus we have

$$\frac{\partial u}{\partial t} + u\frac{\partial u}{\partial x} + v\frac{\partial u}{\partial y} = u_\infty \frac{du_\infty}{dx} + \frac{\mu_{nf}}{\rho_{nf}}\left(1+\frac{1}{\beta}\right)\left(\frac{\partial^2 u}{\partial y^2}\right) - \frac{\nu_{nf}}{K_1}(u-u_\infty) - \frac{\sigma_{nf}B_0^2}{\rho_{nf}}(u-u_\infty) \tag{13}$$

$$\frac{\partial T}{\partial t} + u\frac{\partial T}{\partial x} + v\frac{\partial T}{\partial y} = \frac{k_{nf}}{(\rho C_p)_{nf}}\frac{\partial^2 T}{\partial y^2} + \frac{\mu_{nf}}{(\rho C_p)_{nf}}\left(1+\frac{1}{\beta}\right)\left(\frac{\partial u}{\partial y}\right)^2 + (T-T_\infty)\frac{Q_0}{(\rho C_p)_{nf}} \tag{14}$$

New self-similarity variables are as follows:

$$\eta = \lambda\left(\frac{y}{x}\right),$$
$$f\left(\eta,\tau^*\right) = \frac{\psi\left(x,y\right)}{\lambda\alpha^*},$$
$$u = \frac{bx^m}{\left(1+\mathrm{Pr}\right)^{2n}}\left(\frac{\partial f\left(\eta,\tau^*\right)}{\partial\eta}\right),$$
$$v = -\lambda\left(\frac{\alpha^*}{x}\right)\left[f\left(\eta,\tau^*\right)\frac{m+1}{2} + \eta\frac{\partial f\left(\eta,\tau^*\right)}{\partial\eta}\frac{m-1}{2} + \tau^*\frac{\partial f\left(\eta,\tau^*\right)}{\partial\eta}\left(m-1\right)\right],$$
$$\tau^* = \frac{bx^{m-1}}{\left(1+\mathrm{Pr}\right)^{2n}}t,$$
$$V_w = -\left(\frac{\alpha^*}{x}\right)\lambda\left[f_w\left(m+1\right)\left[0.5\right]\right],$$
$$T = \left(T_w - T_\infty\right)\theta\left(\eta,\tau^*\right) + T_\infty. \tag{15}$$

By employing new similarity variables, Eqns. (13) – (14) can be written as

$$\left(1+\frac{1}{\beta}\right)\mathrm{Pr}\,F'''A1 + \left(\frac{m+1}{2}\right)\left(f_0F'' + Ff_0''\right) - 2mf_0'F' + \gamma F' - A1K_a\,F'\left(1+\mathrm{Pr}\right)^{2n} - \frac{\sigma_{nf}}{\sigma_f}\frac{M_a}{A2}F'\left(1+\mathrm{Pr}\right)^{2n} = 0 \tag{16}$$

$$\frac{k_{nf}}{k_f}\frac{1}{A3}S'' + \left(\frac{m+1}{2}\right)\left(f_0S' + F\theta'\right) + \gamma S + \frac{\mathrm{Pr}\,E_c}{\left(1+\mathrm{Pr}\right)^{2n}}\frac{f_0''F''}{A4} + \frac{QS}{A3}\left(1+\mathrm{Pr}\right)^{2n} = 0 \tag{17}$$

appropriate boundary conditions:

$$f\left(0,\tau^*\right) = f_w, f'\left(0,\tau^*\right) = \lambda_T\left(1+\mathrm{Pr}\right)^{2n}, \theta\left(0,\tau^*\right) = 1 \text{at } \eta = 0,$$
$$f'\left(\eta,\tau^*\right) = \left(1+\mathrm{Pr}\right)^{2n}, \theta\left(\eta,\tau^*\right) \to 0, \quad \text{as } \eta \to \infty \tag{18}$$

by using the below perturbation expressions stability test is executed

with $f = f_0\left(\eta\right)$ and $\theta = \theta_0\left(\eta\right)$.

$$f\left(\eta,\tau^*\right) = f_0\left(\eta\right) + e^{-\gamma\tau^*}F\left(\eta\right),$$
$$\theta\left(\eta,\tau^*\right) = \theta_0\left(\eta\right) + e^{-\gamma\tau^*}S\left(\eta\right). \tag{19}$$

Along with the boundary conditions

$$F\left(\eta\right) = 0, F'\left(\eta\right) = 0, S\left(\eta\right) = 0 \quad \text{at } \eta = 0,$$

$$F'(\eta)=0, S(\eta)\to 0, \qquad \text{as } \eta\to\infty \tag{20}$$

By numerically resolving the eigen value problem for particular values of Q = 0.01, Ec = 0.01, Pr = 6.2, Ka = 0.01, fw = 2.5 and Ma = 0.01 an infinite set ($\gamma_1 < \gamma_2 < \gamma_3 <$ .....) of eigen values can be determined. When γ is positive, the solution is steady; when γ is negative, the solution is unsteady. According to Harris et al. [42], normalization of an appropriate boundary condition on $F(\eta)$ or $S(\eta)$ is required to determine the eigen values. The condition $F'(\eta)\to 0$ as $\eta\to 0$ is normalized in the current exemplar. and the new condition F″ (0) = 1 is used to elucidate the flow equations.

NUMERICAL EXPLANATION:

The bvp4c collocation formula in MATLAB is used to resolve the dimensionless set of nonlinear equations (7) and (8) with the ensuing boundary conditions [Eq. (9)], with a degree of error tolerance of 10-6. A MATLAB package called Bvp4c gives the answer using the finite difference method and the three-stage Lobatto III a formula.

Table 2 compares the current results with Lin and Lin without $\phi, K_a, F_r, and\ Ec$ for the second solution. As can be observed, the current results are fairly consistent with the comparison results.

TABLE 2: Comparison result of Nu^* in the absences of $\phi, K_a, F_r, and\ Ec$ with the results of Lin and Lin for second solution.

Pr	Wedge		Stagnation Point	
	Lin and Lin [39]	Present Results	Lin and Lin [39]	Present Results
0.01	0.61437	0.61025	0.76098	0.76002
0.1	0.55922	0.55871	0.70524	0.70762
1	0.49396	0.49453	0.64032	0.64193
10	0.47703	0.47003	0.63192	0.63234

RESULTS AND DISCUSSION:

This section illustrates and analyses the effects of different physical factors on skin friction (C^*_f), Nusselt number (Nu^*), velocity (f′), temperature *(θ),* and in stretching or compressing wedge and stagnation point situations with porous media. Bvp4c has been used to calculate the dimensionless equations of the flow field with appropriate border conditions. It is

noteworthy to analyse the transit characteristics over a wedge (β_1= 0.5) and stagnation point (β_1= 1.0).

With the stretching or compressing wedge and stationary point surfaces, twin solutions are attained. Therefore, the main goal is to identify the critical points in the two solutions that correlate to the emerging parameters. To determine which of the twin solutions is steady, a stability check is carried out. Additionally, the first and second solutions are represented by the dashed and solid lines, respectively.

The dual nature of the graphene/H_2O nanofluid flow is illustrated in Figures 2–7 for diverse values of the expanding/contracting surface constant (λ_M) over wedge and stagnation point situations. The first and second solutions subsist for $\lambda_M > \lambda_c$, there is only one solution for $\lambda_M = \lambda_c$ and there are no solutions for $\lambda_M < \lambda_c$, where lower script '*c*' represents the critical value.

Figures 2(a) and 2(b) depict variations in skin friction (C_f^*) for both geometries with λ_M and suction/injection parameter (f_w). As can be seen in the figure that there are triple solutions for $\lambda_M < \lambda_c < 0$ where the crucial values for the wedge cases are $\lambda_c \approx$ -1.331, -1.408, and -1.490 and for the stagnation point cases are $\lambda_c \approx$ -1.639, -1.735, and -1.835. Additionally, C_f^* and f_w are directly proportional for the first solution but it deteriorate for the other solution

The effects of the Casson parameter (β) and the extending/contracting surface parameter (λ_M) on skin friction are shown in Figures 3(a) and 3(b). It can be seen that the critical values for the wedge and stagnation point are $\lambda_c \approx$ -1.331, -1.338, and -1.340, and $\lambda_c \approx$ -1.639, -1.644, and -1.648 for rising values of β = 6.0, 7.0, and 8.0. Critical point value goes up with higher numbers of β. Furthermore, for larger values of β, the nature of the primary and secondary solutions is reversed on C_f^* .

Figures 4(a) and 4(b) show how the rate of heat transmission (Nu^*) varies with (λ_M) as Eckert number escalate. These figures show that there are two possibilities for a given value of λ_M when $\lambda_M \leq \lambda_c$. For increasing values of Ec = 0.01, 0.03, and 0.05, the critical values of λ_M are $\lambda_c \approx$ 1.331, 1.338, and 1.340 over a wedge and $\lambda_c \approx$ 1.639, 1.620, and 1.565 over a stagnation point. Moreover, one finds that Nu^* of nanofluid for the two different geometries

improves for rising λ_M. However, for both solutions, a rise in EC limits the enhancement of Nu^* at the surface.

Changes in Nu^* due to M_a with λ_M are represented in Fig. 5(a, b). It is significant to observe that these figures contain the critical points information for the values of M_a, $\lambda_c \approx$ -1.315, -1.321, -1.330 and $\lambda_c \approx$ -1.639, -1.644, -1.650, for both situations. The solutions appears that the first portrays a diminishing nature, whereas the second upsurge for Nu^* at the surface for strong M_a.

Figures 6(a,b) discloses the surface parameter expansion/contraction effect (λ_M) on Nu^* with Heat source/sink (Q). It has been observed that Nu^* improves for rising λ_M or both the cases. However, a rise in Q limits the surface-level increases of Nu^* for both the solutions.

The favorable and unfavorable values of γ_1 the primary and secondary approaches are depicted in Figures 7(a) and 7(b). The second approach on the two cases are shown to be stable, whereas the another approach is shown to be unstable.

The impact of λ_M on skin friction (C_f^*) against f_w for the twin solutions over the two cases, is explored in Figures 8(a,b) and 9(a,b). It should be mentioned that the contour graphs are plotted using 50 x 50 mesh points. These figures demonstrate that for greater values of λ_M on skin friction, both the solutions behave differently.

Figures 10(a, b) and 11(a, b) show the effect of λ_M on Nusselt Number ($Nu*$) with Ec for both the cases and noted that a high heat transfer rate for the two surfaces for reduced eigen values.

Sketches of 12(a,b) and 13(a,b) are shown to illustrate the effects of suction or injection (f_w) on f' and θ. The performance of f_w on f' is put on view in figure 12(a,b). A raise in velocity of the Casson nanofluid is observed with injecting of the fluid into the surface. In reality, when injection of the fluid increases the thickness of the boundary layer increases the fluid movement close to the outer surface however the first solution is found to have the opposite nature. The consequences of f_w on temperature is represented in Fig. 13(a,b). It is spotted that the temperature of the nanofluid increase by increasing f_w for the stable case. Furthermore, it

should be mentioned that injecting fluid at the surface results in a reduction in the thickness of the thermal boundary layer. The temperature of the Casson nanofluid consequently drops.

The variations in f' and θ are shown in Figs. 14(a,b) and 15(a,b) for larger values of the Casson parameter (β) in both situations. The elevating values of β are demonstrated in Figure 14(a,b). The Casson nanofluid's viscosity declines and exhibits a decreasing behaviour in temperature profile can be seen from the figure 15 (a,b) under the impact of buoyancy force. The thickness of the temperature boundary layer also decreases as the value of the Casson fluid parameter rises. The thermal barrier layer, however, thins as elasticity stress variable increases. It is evident that the lower thermal diffusivity values associated with the slimmer thermal boundary layer correspond to a greater temperature gradient in the vicinity of the two geometries.

When examining the features of velocity and temperature, the porous permeability parameter (Ka) is crucial. Figures 16(a) and 16(b) reveal that in the case of second solution, the velocity shoot up for ascending Ka. The permeability of the porous medium rises with an increase in Ka, results velocity go up. It is observed that the fluid's permeability and the Darcian force are exhibiting opposite natures. As a result, in the first solution case, the flow in the boundary layer is interrupted. Figures 17 (a) and 17 (b) show how Ka affects temperature for the first and second solutions, respectively. This figure shows that, for the second solution, the nanofluid temperature plumnets with a rise in Ka, whereas it climbs for the first solution.

Figures 18(a,b) and 19(a,b) show how the magnetic field () affects the velocity and temperature curves. The relationship between the velocity and the rise in the magnetic field parameter is shown to be negative in Fig. 18(a,b). Motion of a substance is affected by a magnetic field. When an attracting field is introduced, fluid particles chain together and move in that direction. When particles and liquids interact, a barrier is formed that restricts the movement of the liquids.

As the viscosity rises, the fluid rate falls. Thus, a decrease in the velocity profile results from a rise in the magnetic field. Figure 19(a,b) shows that M_a and temperature distribution are conversely related to one another. This is due to the fact that an increase in magnetic number increases magnetic force and weakens the convective heat transfer mechanism by expanding the magnetic field strength. Convection is less effective at higher magnetic field strengths. As a

consequence, movement of the fluid decreases results in conduction as the foremost heat transfer means.

The Ecker number (Ec) on temperature curve for both wedge and stagnation point flow is illustrated in Figure 20(a,b). It can be concluded that for both cases, the temperature rises as Ec increases. In practice, the temperature rises due to the small impact of the enthalpy difference, because the Eckert number $Ec = \frac{u_\infty^2}{C_p\left(T_w - T_\infty\right)}$ is defined as the fraction of kinetic energy flow and the enthalpy difference within the boundary layer. This causes kinetic energy to be converted into internal energy by dissimilar fluid tension.

Figure 21(a,b) depicts the effect of the heat production or absorption parameter (Q) on the temperature profile. The temperature field increases as Q increases in both situations, as shown in Figure. In addition, as Q rises, so does the thickness of the thermal boundary layer. More temperature usually comes out into the working fluid during the heat generation process. As a result, as the heat generation parameter rises, so does the temperature profile. Furthermore, the temperature field rises as a result of exothermic chemical processes.

SUMMARY AND CONCLUSIONS

The purpose of this research was to investigate the double natures and stable behavior of graphene/H_2O nanofluid flow across an expanding or contracting wedge and stagnation point using the Casson model. At the border condition, the surface underwent suction/injection with viscous dissipation. two solutions are observed in a particular region when the wedge and stationary point surface are expanded/contracted. The most important closing remarks are given below.

- The permeability causes the two solutions to behave differently with respect to velocity.
- For greater Casson parameter β both the solutions are contradictory on C_f^*.
- The Nu^* of the fluid at the two surfaces advances for raising λ_M and decreases for Eckert number
- As Q increases, the temperature field increases for both the cases.
- Physical intuition dictates that the second option is the more stable one.
- Uplifting values of β elevate velocity and decrement in temperature.

References

1. Ghasemi, S.E., Hatami, M., Ganji, D.D..Analytical thermal analysis of air-heating solar collectors, *J. Mech. Sci. Technol*. 2013; 27 (11): 3525–3530.
2. Nasrin, R., Alim, M.A.. Dufour-soret effects on natural convection inside a solar collector utilizing water-cuo nanofluid, *International Journal of Energy & Technology*. 2012; 4 (23): 1–10.
3. Harada, N., Tsunoda, K.. Study of a disk MHD generator for nonequilibrium plasma generator (NPG) system, *Energy Convers. Manag*. 1998; 39 : 493–503.
4. Shang, J.S.,. Recent research in magneto-aerodynamics, *Prog. Aero. Sci*. 2001;37 : 1–20.
5. Ghasemi, S.E., Hatami, M.. Solar radiation effects on MHD stagnation point flow and heat transfer of a nanofluid over a stretching sheet, *Case Studies in Thermal* ***Engineering*** 2021; 25: 100898.
6. Thirupathi, T., Vusi Mpendulo Magagula. Transient electromagnetohydrodynamic radiative squeezing flow between two parallel Riga plates using a spectral local linearization approach, *Heat Transfer–Asian Res*. 2020; 49 (1) :67–85.
7. Bala Anki Reddy, P and Suneetha, S. Impact of Cattaneo-Christov Heat Flux In the Casson Fluid Flow Over a Stretching Surface With Aligned Magnentic Field and Homogeneous Heterogeneous Chemical Reaction, *Frontiers in Heat and Mass Transfer* . 2018.
8. Lund, Liaquat Ali, et al. Dual similarity solutions of MHD stagnation point flow of Casson fluid with effect of thermal radiation and viscous dissipation: stability analysis." *Scientific reports.* 2020;10(1) : 1-13.
9. Hussain, Azad, et al., MHD stagnation point flow of a Casson fluid with variable viscosity flowing past an extending/shrinking sheet with slip effects. *Physica A: Statistical Mechanics and Its Applications.*2020*;* 553 : 124080.
10. Casson, N., *A flow equation for the pigment oil suspensions of the printing ink type, Rheology of Disperse Systems*, Pergamon, New York. 1959; 84-102.
11. Mythili, D., Sivaraj, R. Influence of higher order chemical reaction and non-uniform heat source / sink on Casson fluid flow over a vertical cone and flat plate, *Journal of Molecular Liquids*. 2016; 216: 466–475.
12. Bala Anki Reddy, P., Suneetha,S., Subbarayudu, K., Al-Arabi T.H. & Rashad A.M. Exploration of physical features of homogeneous–heterogeneous chemical action in a nanofluid film dispensed with MOS2 in diathermic oils, *Journal of Taibah University for Science.* 2021; 15,1: 826-839.
13. Wahidunnisa, L., Suneetha, S., Reddy, S.R.R., Bala Anki Reddy, P.. Comparative study on electromagnetohydrodynamic SWCNT-water dusty nanofluid in the presence of radiation and Ohmic heating, *Proceedings of the Institution of Mechanical Engineers, Part E: Journal of Process Mechanical Engineering*. 2021;1-9.

14. Suneetha, S., Subbarayudu, K., Bala Anki Reddy, P.. Model for navier's slip boundary condition flow of nanofluid past a non-linear stretching sheet with Soret effect**,** *Engineering Transactions*. 2020; 68(2) :177–198.
15. Sreedevi, P., Sudarsana Reddy, P. Heat and mass transfer analysis of MWCNT's kerosene nanofluid flow over a wedge with thermal radiation. *Heat Transfer.* 2020;1-24.
16. Khan N.S., Kumam P., Thounthong P.. Second law analysis with effects of Arrhenius activation energy and binary chemical reaction on nanofluid flow, *Scientific Reports*. 2020; 10, 1226.
17. Suneetha, S., Subbarayudu, K, Bala Anki Reddy,P., Chamkha, A.J. Numerical investigation of non-Fourier flux theory with chemical action on Maxwell radiating nano liquid: A biomedical application, *Lecture Notes in Mechanical Engineering book series*, 2020; 793-810.
18. Buongiorno, J. Convective Transport in Nanofluids, *Journal of Heat Transfer*, 2006; 128: 240.
19. Muhammad Arif, Suneetha,S., Thameem Basha, Bala Anki Reddy,P., Poom Kumam. Stability analysis of diamond-silver-ethylene glycol hybrid based radiative micropolar nanofluid: A solar thermal application, *Case Studies in Thermal Engineering.* 2022; 39.
20. Wahidunnisa, L., Suneetha, S., Reddy, S.R.R., Bala Anki Reddy, P.. Comparative study on electromagnetohydrodynamic SWCNT-water dusty nanofluid in the presence of radiation and Ohmic heating, *Proceedings of the Institution of Mechanical Engineers, Part E: Journal of Process Mechanical Engineering*. 2021; 1-9.
21. Suneetha, S., Wahidunnisa, L., Divya, A., and Bala Anki Reddy,P. Electrical magnetohydrodynamic flow of kerosene oil based carbon nanotube's Maxwell nanofluid in the presence of non-linear radiation and Cattaneo-Christov heat diffusion: Applications in aerospace industry, *Proc Mech E, Part E: J Process Mechanical Engineering*. 2022; 1–9.
22. Venkateswarlu, A, Suneetha, S. Jayachandra Babu, M, Girish Kumar,J, Raju CSK and Qasem Al-Mdallal. Significance of Magnetic Field and Chemical Reaction on the Natural Convective Flow of Hybrid Nanofluid by a sphere with viscous dissipation: A statistical Approach, *Nonlinear Engineering*, 2021; 10:563–573. https://doi.org/10.1515/nleng-2021-0047
23. Subbarayudu, K. Suneetha, S, Bala Anki Reddy,P. The assessment of time dependent flow of Williamson fluid with radiative blood flow against a wedge, *Propulsion and power research*, 2020, 9(1), 87-99 , **d**oi.org/10.1016/j.jppr.2019.07.001. ISSN: 2195-4356.
24. Thameem Basha, H & Sivaraj, R. On The Stability Of Copper Oxide/Water Non-Darcy Nanofluid Flow Over An Extending/Contracting Wedge And Stagnation Point, *Special Topics & Reviews in Porous Media* — An International Journal, 2020; 11(X):1–20.
25. Basha, H. Thameem, Sivaraj, R. and Isaac Animasaun, L. Stability analysis on Ag-MgO/water hybrid nanofluid flow over an extending/contracting Riga wedge and

stagnation point." *Computational Thermal Sciences: An International Journal*. 2020;12.6.

26. Radha Madhavi, M. Sridhar, W. and Puvvada Nagesh, Numerical investigations of MHD Casson nanofluid flow over a wedge through porous medium, *AIP Conference Proceedings* ,2021; **2375**, 030011. https://doi.org/10.1063/5.0066944
27. K. Hiemenz, Dinglers Polytechnic J. 1911; 326 -321.
28. Bala Anki Reddy, P. and Suneetha, S. Effects Of Homogeneous-Heterogeneous Chemical Reaction And Slip Velocity On Mhd Stagnation Flow Of A Micropolar Fluid Over A Permeable Stretching/Shrinking Surface Embedded In A Porous Medium, Frontiers in Heat and Mass Transfer (FHMT), 2017; 8, 24 . DOI: 10.5098/hmt.8.24
29. Mabood, F.. Ashwinkumar ,G. P &. Sandeep, N. Effect of nonlinear radiation on 3D unsteady MHD stagnancy flow of Fe_3O_4/graphene–water hybrid nanofluid, International Journal of Ambient Energy. 2022; 43:1, 3385-3395. DOI: 10.1080/01430750.2020.1831593.
30. Hassan Waqas, Shan Ali Khan, Taseer Muhammad, Syed Muhammad Raza Shah Naqvi, Heat transfer enhancement in stagnation point flow of ferro-copper oxide/water hybrid nanofluid: A special case study, Case Studies in Thermal Engineering.2021; 28,101615. https://doi.org/10.1016/j.csite.2021.101615.
31. Nurul Amira Zainal, Iskandar Waini, Najiyah Safwa Khashi'ie, Abdul Rahman Mohd Kasim, Kohilavani Naganthran, Roslinda Nazar, Ioan Pop, Stagnation point hybrid nanofluid flow past a stretching/shrinking sheet driven by Arrhenius kinetics and radiation effect, Alexandria Engineering Journal, 2023; 68:29-38. https://doi.org/10.1016/j.aej.2023.01.005.
32. Yangyang Yu, Umair Khan, Aurang Zaib, Anuar Ishak, Iskandar Waini, Zehba Raizah, Ahmed M. Galal, Exploration of 3D stagnation-point flow induced by nanofluid through a horizontal plane surface saturated in a porous medium with generalized slip effects, Ain Shams Engineering Journal.2023;14(2), 101873, https://doi.org/10.1016/j.asej.2022.101873.
33. Manasa M. Biswal, Bharat K. Swain, Manjula Das, Gouranga Charan Dash, Heat and mass transfer in MHD stagnation-point flow toward an inclined stretching sheet embedded in a porous medium, Heat Transfer. 2022; 51(6): 4837-4857. https://doi.org/10.1002/htj.22525.
34. Mahmood, Z., Alhazmi, S.E., Alhowaity, A. *et al.* MHD mixed convective stagnation point flow of nanofluid past a permeable stretching sheet with nanoparticles aggregation and thermal stratification. *Sci Rep.* 2022*;* 12,16020. https://doi.org/10.1038/s41598-022-20074-1.
35. Zainal, N.A.; Nazar, R.; Naganthran, K.; Pop, I. Stability Analysis of Unsteady Hybrid Nanofluid Flow over the Falkner-Skan Wedge. Nanomaterials. 2022; *12*,1771. https://doi.org/10.3390/nano12101771.

36. Cedric Gervais Njingang Ketchate, Pascalin Tiam Kapen, Didier Fokwa, Ghislain Tchuen,Stability analysis of mixed convection in a porous horizontal channel filled with a Newtonian Al2O3/Water nanofluid in presence of magnetic field and thermal radiation, Chinese Journal of Physics. 2022; 79: 514-530, ISSN 0577- 9073. https://doi.org/10.1016/j.cjph.2022.08.024
37. Swati Mukhopadhyay, Casson Fluid Flow And Heat Transfer over a Nonlinearly Stretching Surface," *Chin. Phys. B.* 2013; **22**(7), 0747015 https://doi.org/10.1088/1674-1056/22/7/074701
38. Pramanik S., Casson fluid flow and heat transfer past an exponentially porous stretching surface in presence of thermal radiation, Ain Shams Engineering Journal. 2015; **5**(1): 205- 212.https://doi.org/10.1016/j.asej.2013.05.003
39. Lin, H.T., Lin, L.K., Similarity solutions for laminar forced convection heat transfer from wedges to fluids of any Prandtl number, *International Journal of Heat and Mass Transfer*. 1987; 30: 1111–1118.
40. Bachok, N., Ishak, A., and Pop, I.,MeltingHeat Transfer in Boundary Layer Stagnation-Point Flow towards a Stretching/Shrinking Sheet, *Phys. Lett. A.* 2010; 374: 4075–4079.
41. Makinde, O.D., Stagnation Point Flow with Heat Transfer and Temporal Stability of Ferrofluid past a Permeable Stretching/Shrinking Sheet, Defect Diffus. Forum. 2018; 387: 510-522.
42. Harris, S.D., Ingham, D.B., and Pop, I., Mixed Convection Boundary-Layer Flow near the Stagnation Point on a Vertical Surface in a Porous Medium: Brinkman Model with Slip, J. Mol. Liq. 2009; **77**: 267–285.

ACKNOWLEDGEMENTS

The author would like to acknowledge the UGC-Seed Money Research Grant, Yogi Vemana University, Kadapa, A.P., India for financial support. The author declare that she has no conflict of interest to report regarding the present study.

Fig.2(a,b). Impact of λ_M and f_w on C_f^* for both wedge and stagnation point cases

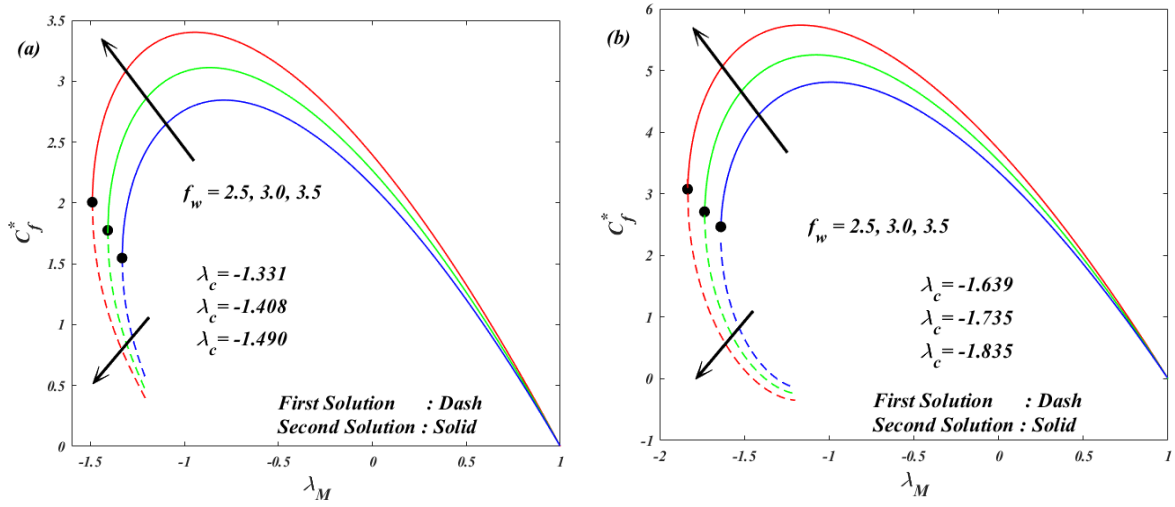

Fig.3(a,b) Impact of λ_M and β on C_f^* for both wedge and stagnation point cases

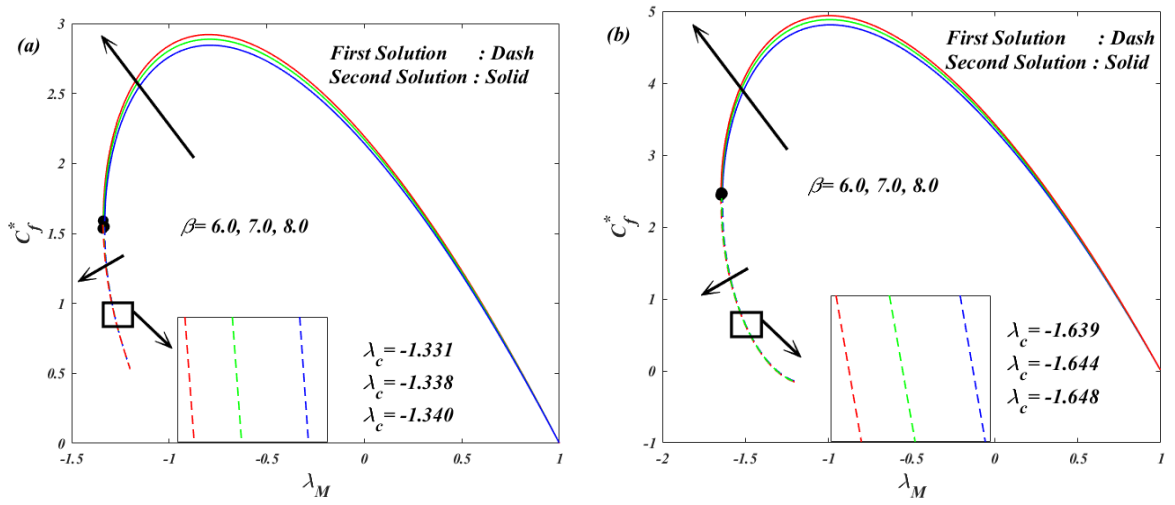

Fig.4(a,b) Impact of λ_M and Ec on Nu^* for both wedge and stagnation point cases

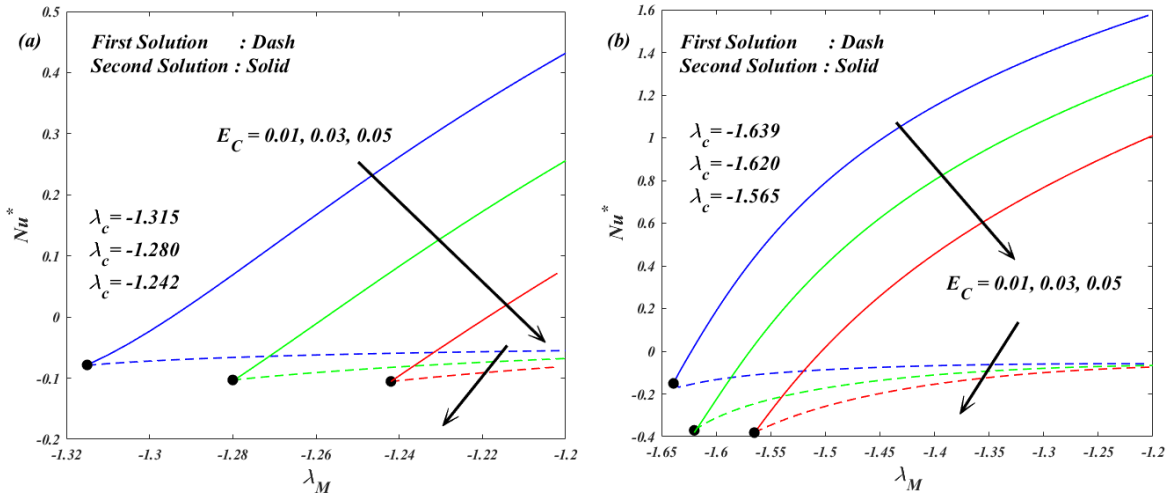

Fig.5(a,b) Impact of λ_M and M_a on Nu^* for both wedge and stagnation point cases

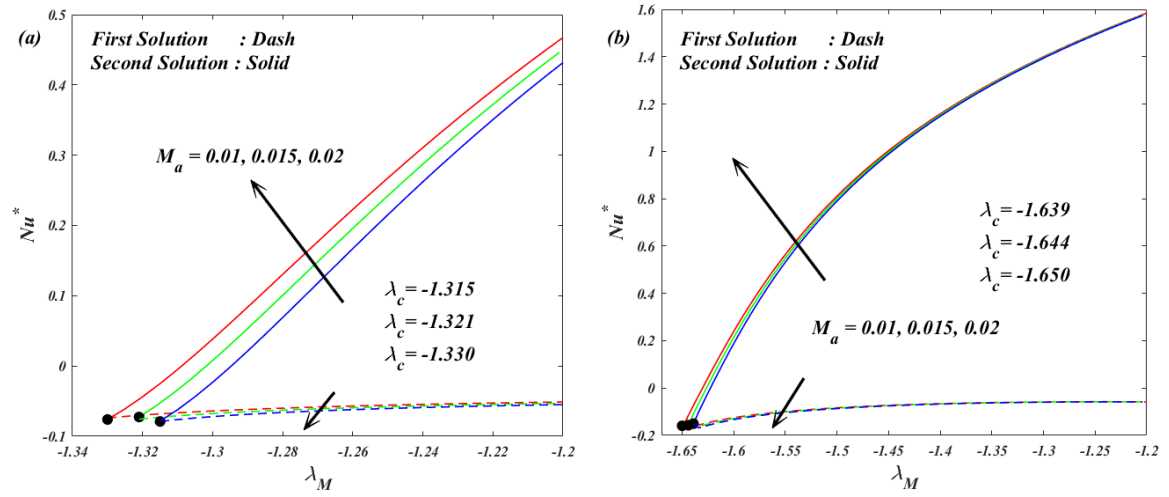

Fig.6(a,b) Impact of λ_M and Q on Nu^* for both wedge and stagnation point cases

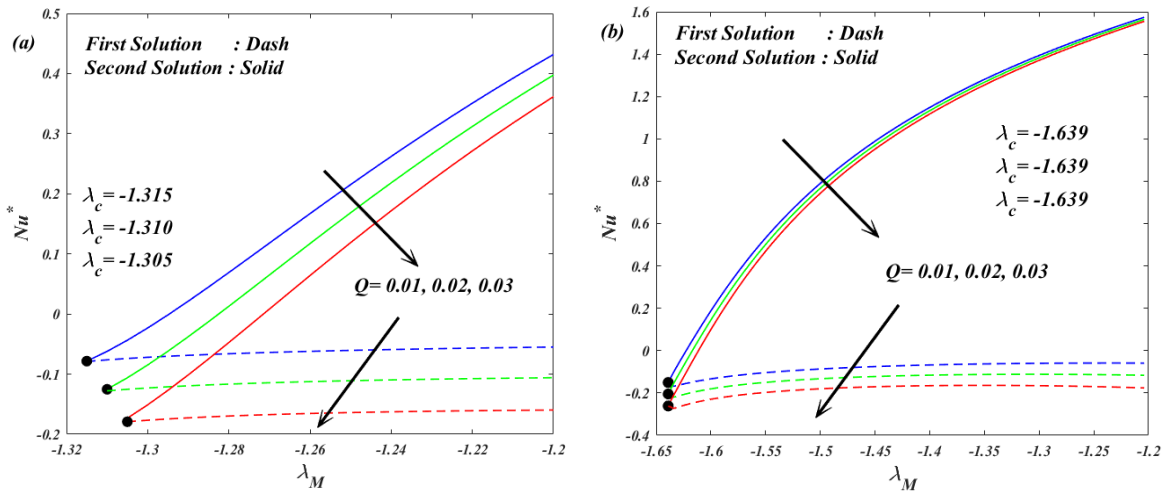

Fig.7(a,b). Plot of smallest eigenvalues for rising λ_M in wedge and stagnation point cases

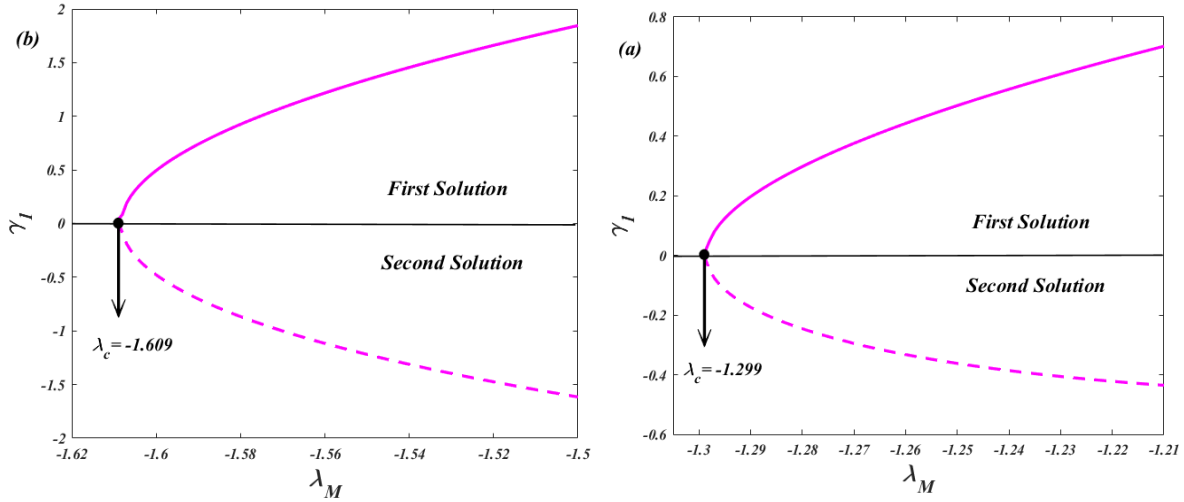

Fig.8. Contour plot with impacts of λ_M and f_w on Skin friction (a) first solution (b) second solution of Wedge case

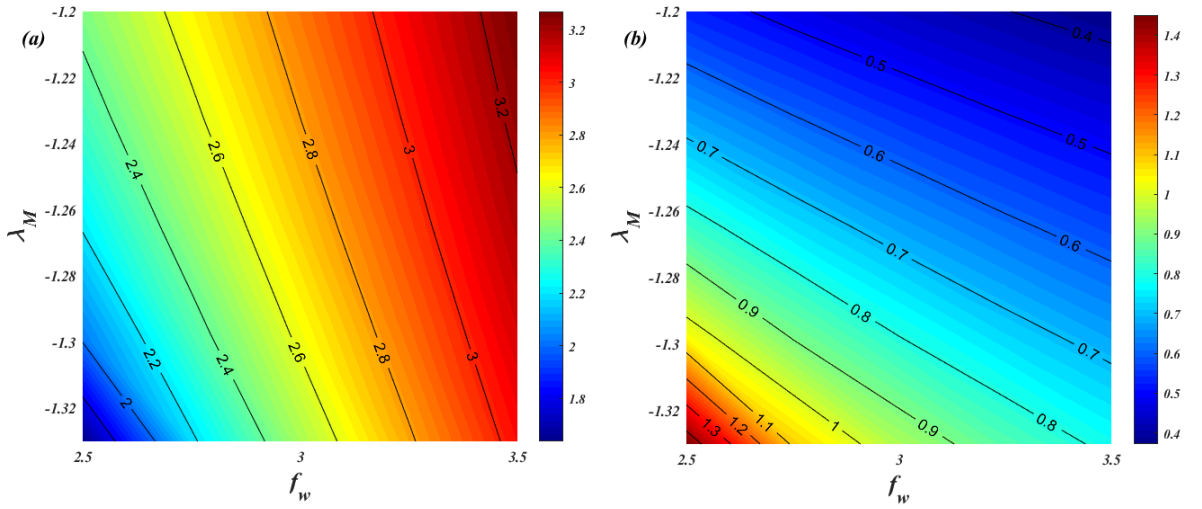

Fig.9. Contour plot with impacts of λ_M and f_w on Skin friction (a) first solution (b) second solution of Stagnation point case

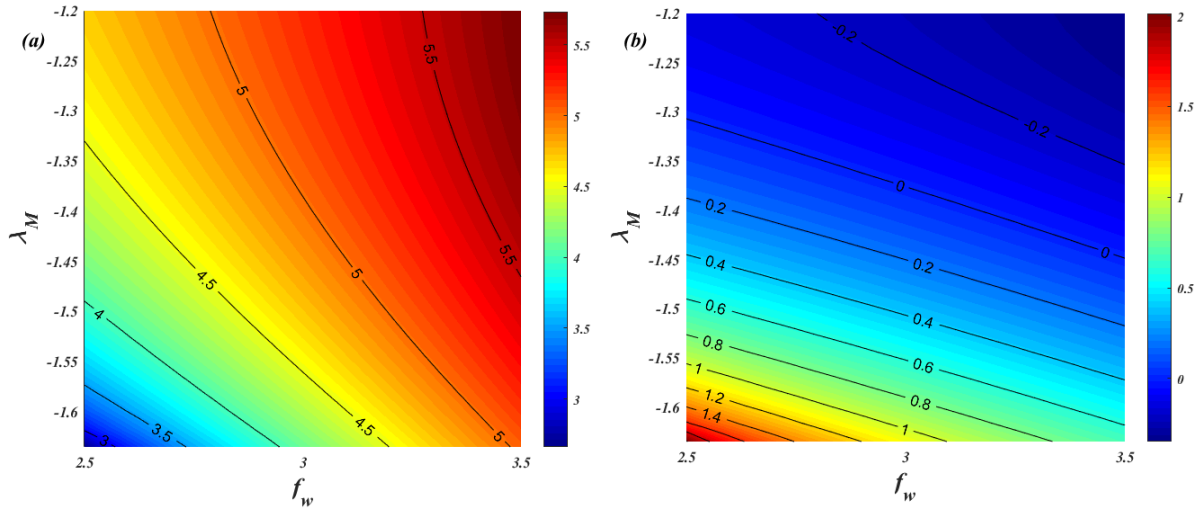

Fig.10. Contour plot with impacts of λ_M and Ec on Nusselt number (a) first solution (b) second solution for wedge case

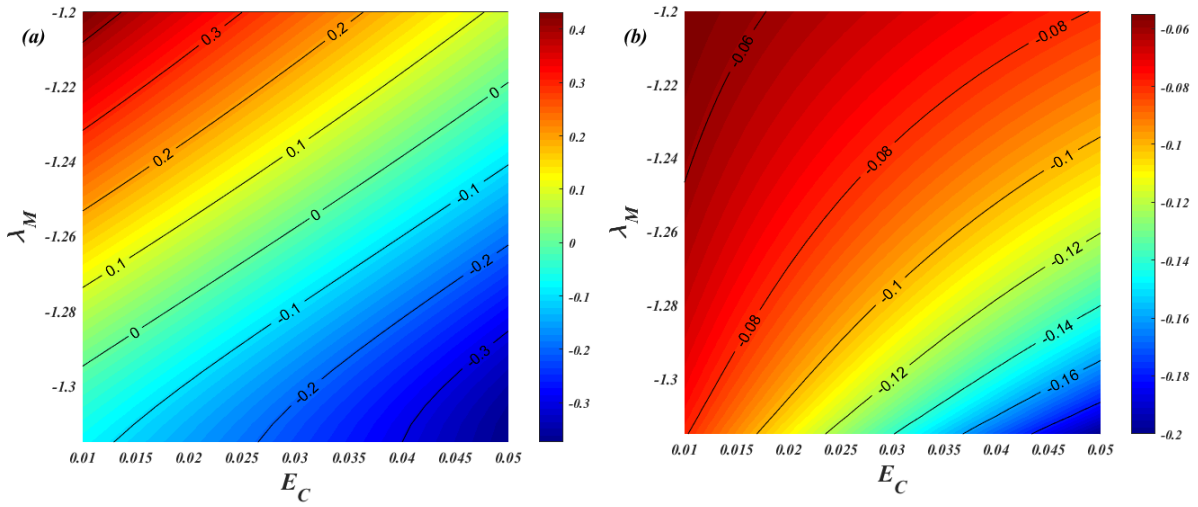

Fig.11. Contour plot with impacts of λ_M and Ec on Nusselt number (a) first solution (b) second solution of Stagnation point case

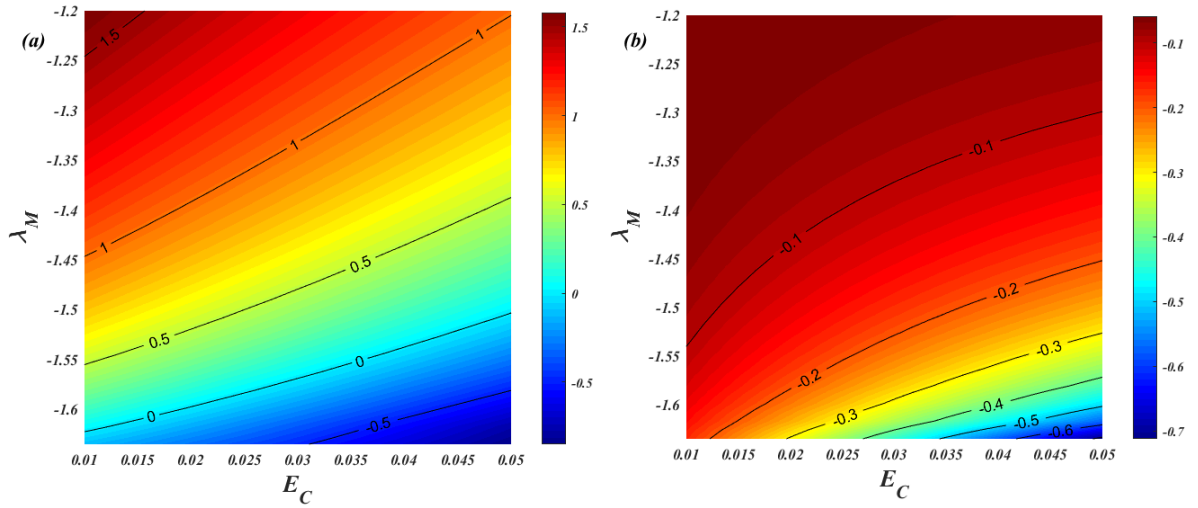

Fig.12(a,b) Plot of f' for increasing f_w for both wedge and stagnation point cases

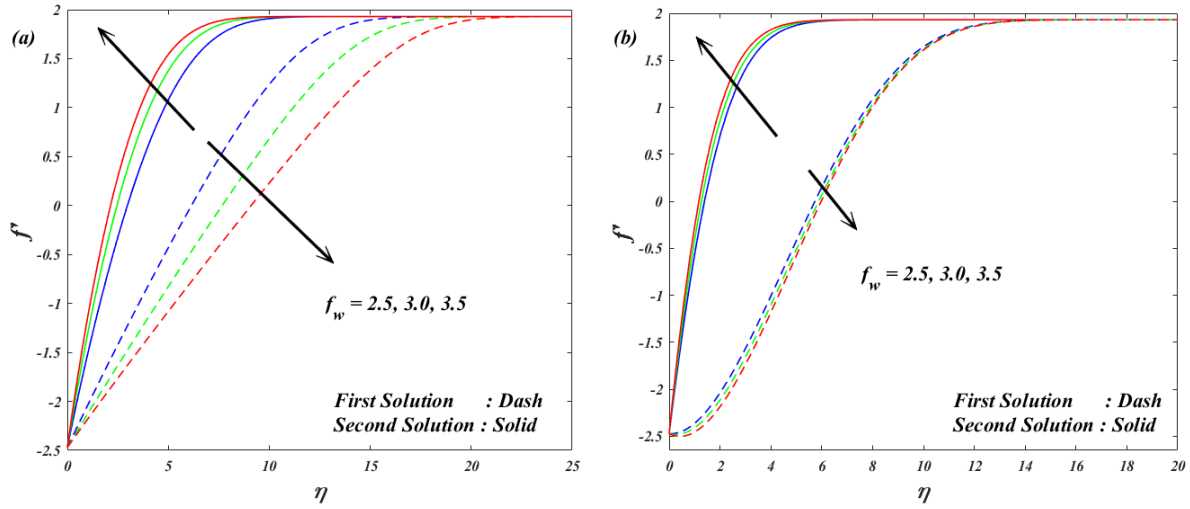

Fig.13(a,b) Plot of θ for increasing f_w for both wedge and stagnation point cases

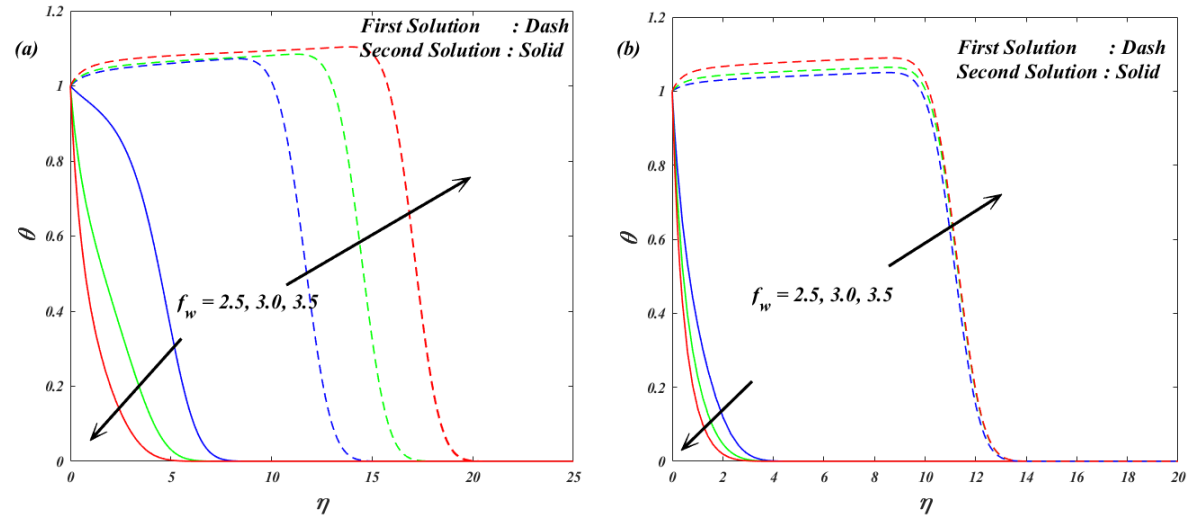

Fig.14 (a,b) Plot of f' for increasing β for both wedge and stagnation point cases

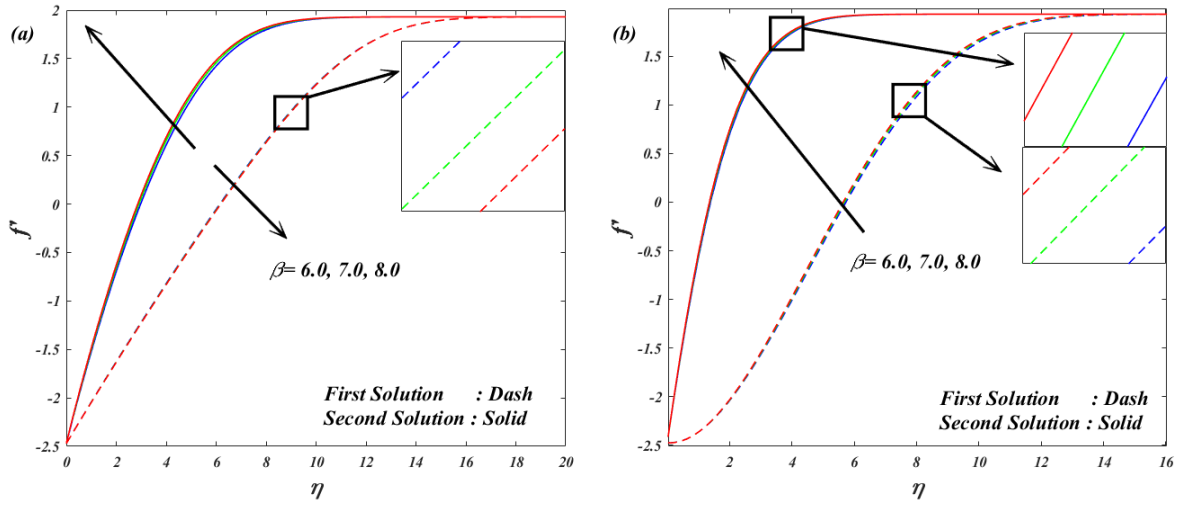

Fig.15 (a,b) Plot of θ for increasing β for both wedge and stagnation point cases

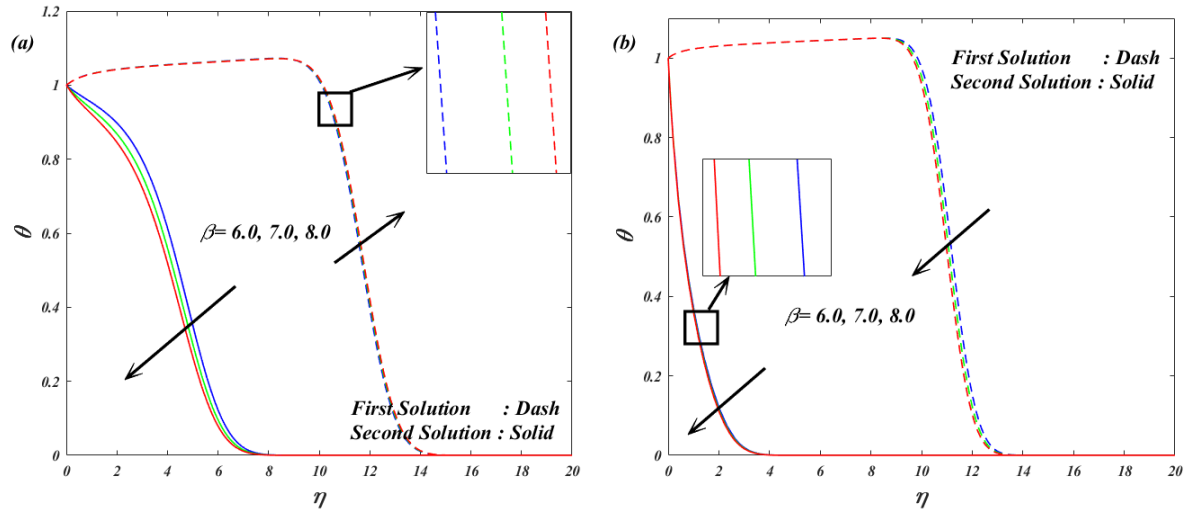

Fig.16 (a,b) Plot of f' for increasing K_a for both wedge and stagnation point cases

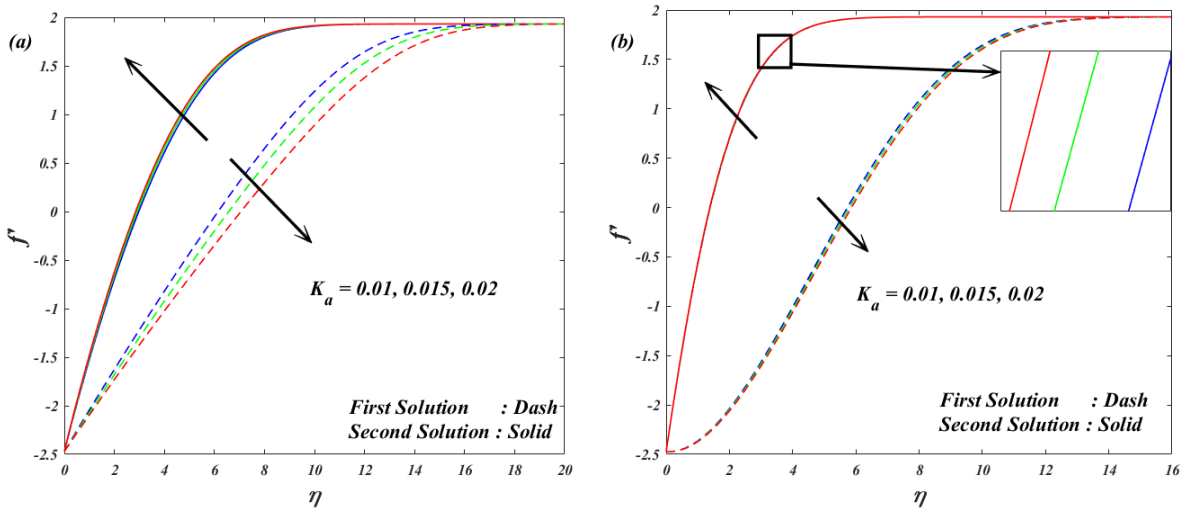

Fig.17 (a,b) Plot of θ for increasing K_a for both wedge and stagnation point cases

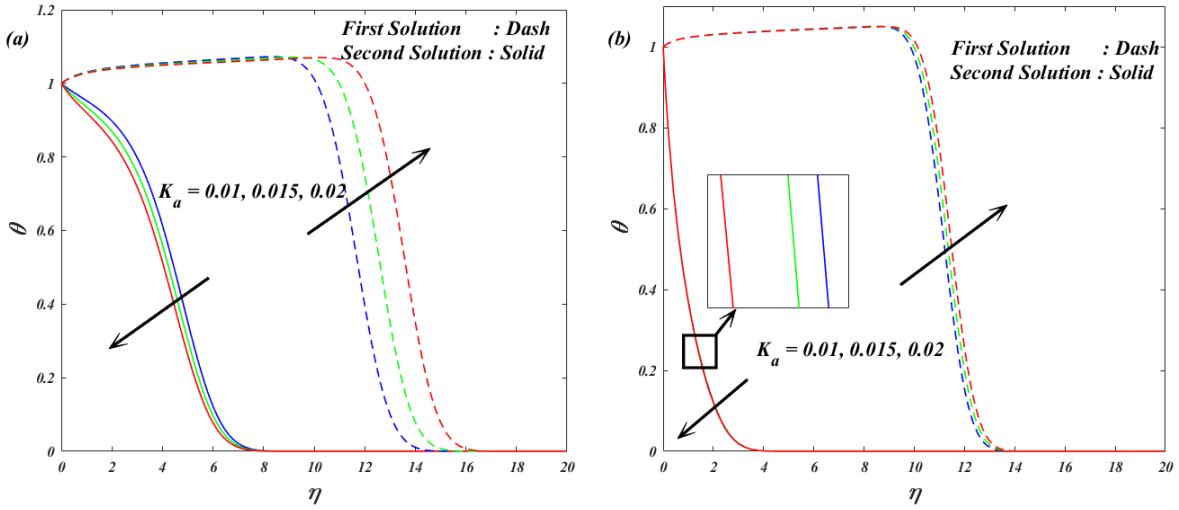

Fig.18 (a,b) Plot of f' for increasing M_a for both wedge and stagnation point cases

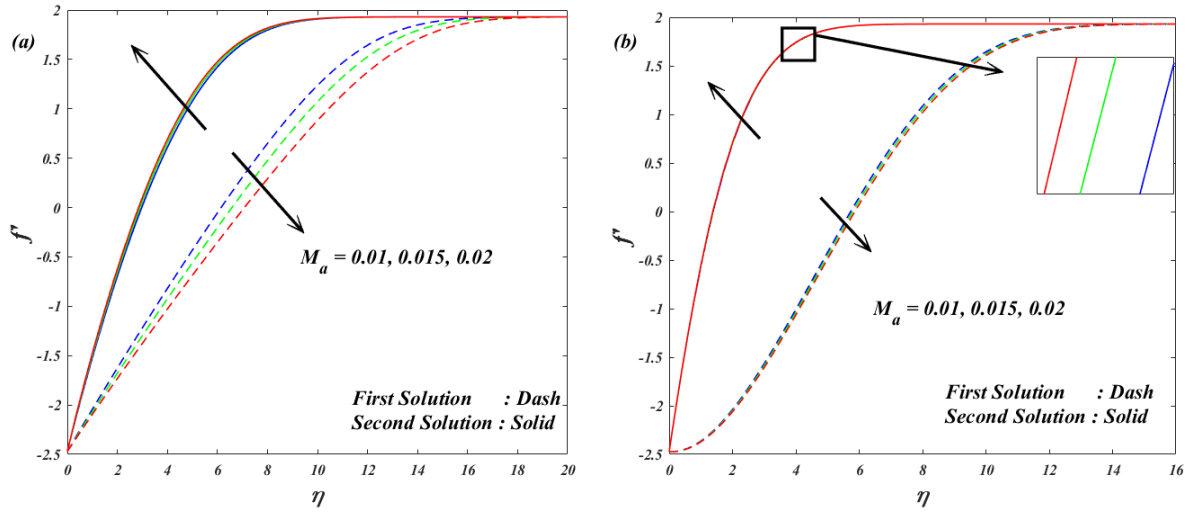

Fig.19 (a,b) Plot of θ for increasing M_a for both wedge and stagnation point cases

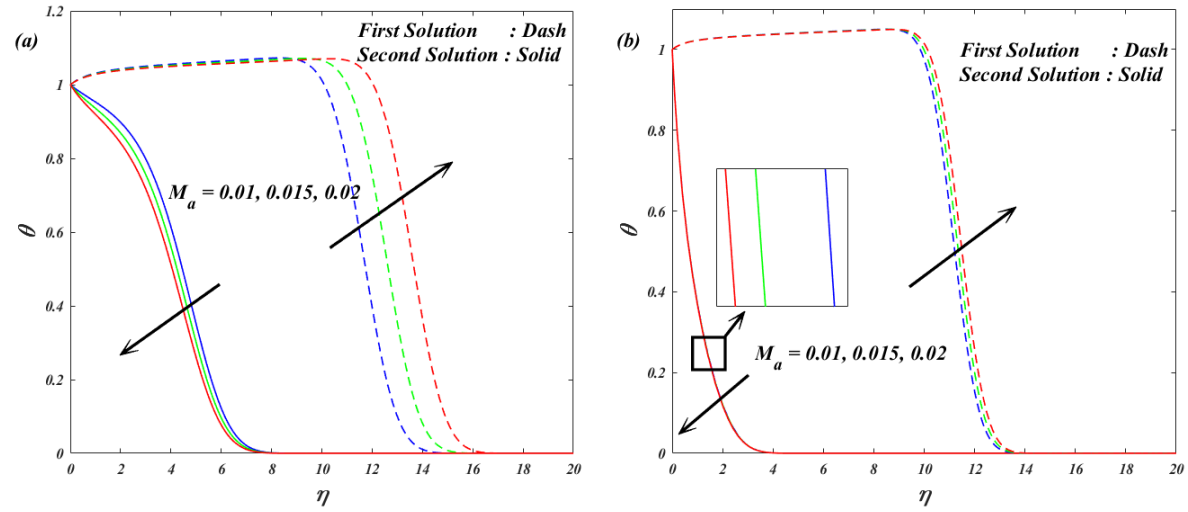

Fig.20 (a,b) Plot of θ for increasing Ec for both wedge and stagnation point cases

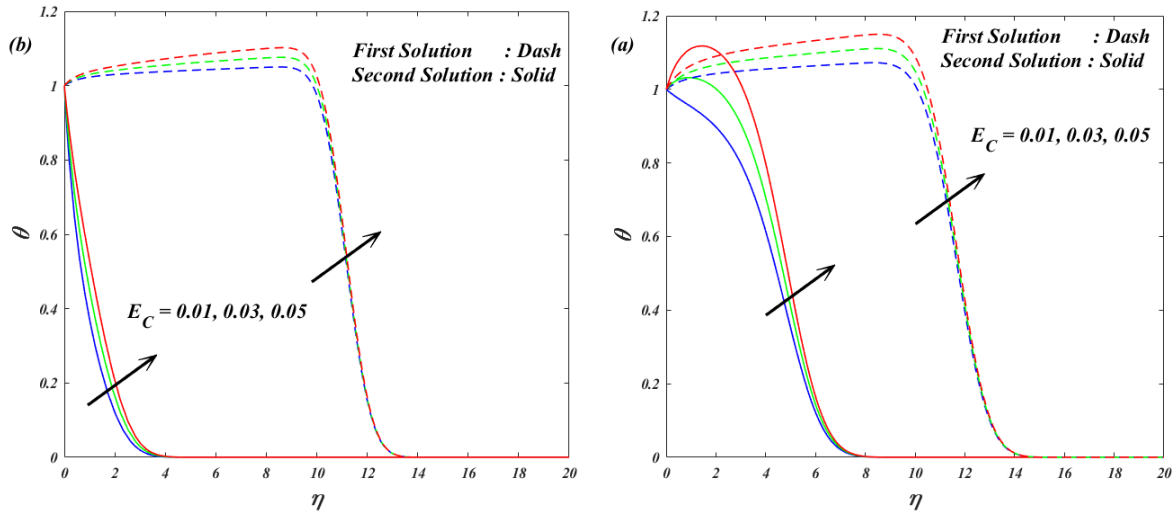

Fig.21 (a,b) Plot of θ for increasing Q for both wedge and stagnation point cases

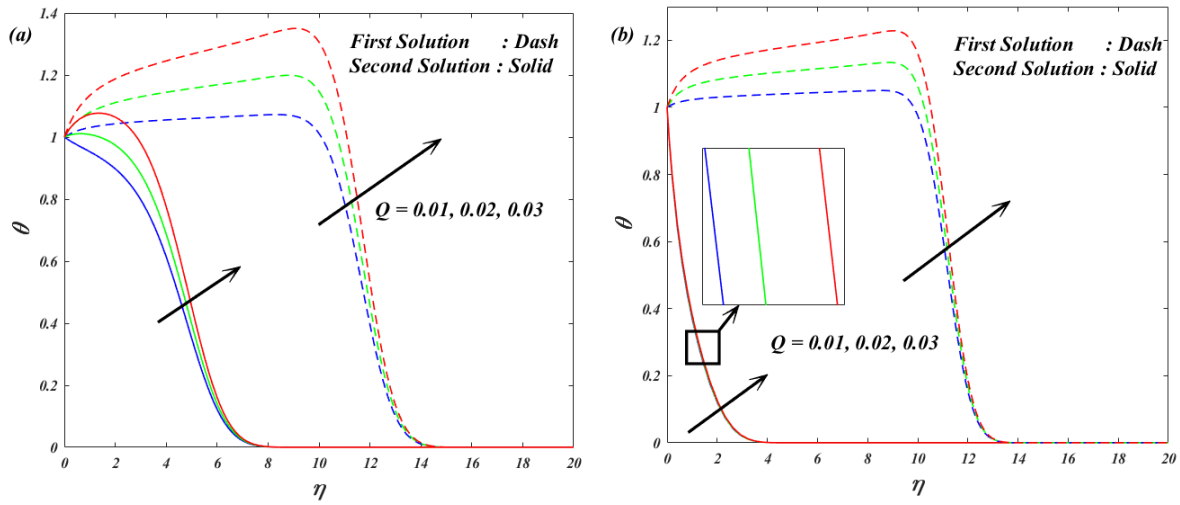

NOMENCLATURE

b constant

C_f^* skin friction coefficient

C_p specific heat capacity

Ec Eckert number

f fluid velocity

f_w suction/injection parameter

K_1 dimensional porous permeability parameter

k_f fluid thermal conductivity

K_a porous permeability parameter

M_a magnetic parameter

m Hartree pressure gradient

Nu^* rate of heat transfer

Pr Prandtl number

Q heat absorption/generation coefficient

Re Reynolds number

T_w wall temperature

T_∞ ambient temperature

u, v the velocity components along the x- and y-directions

x, y Cartesian coordinates

Greek Symbols

α^* thermal diffusivity

β Casson fluid parameter

β_1 angle factor of the wedge

θ dimensionless temperature

μ_f dynamic viscosity

υ_f kinematic viscosity

ρ_f density of fluid